10-15-2018

# First observations of volcanic eruption clouds from the L1 Earth-Sun Lagrange point by DSCOVR/EPIC

Simon Carn
*Michigan Technological University*, scarn@mtu.edu

N. A. Krotov
*NASA Goddard Space Flight Center*

B. L. Fisher
*NASA Goddard Space Flight Center*

C. Li
*NASA Goddard Space Flight Center*

A. J. Prata
*AIRES Pty Ltd*

Geophysical Research Letters

RESEARCH LETTER
10.1029/2018GL079808

**Key Points:**
- Volcanic eruption clouds can be detected and tracked with hourly temporal cadence from L1 orbit
- The hourly cadence of EPIC volcanic $SO_2$ observations can be used to attribute gas emissions to specific events during multiphase eruptions
- Observations of transient variations in $SO_2$ loading will provide more constraints on processes such as $H_2S$ oxidation in volcanic clouds

**Supporting Information:**
- Supporting Information S1
- Movie S1
- Movie S2
- Movie S3

**Correspondence to:**
S. A. Carn,
scarn@mtu.edu

**Citation:**
Carn, S. A., Krotkov, N. A., Fisher, B. L., Li, C., & Prata, A. J. (2018). First observations of volcanic eruption clouds from the L1 Earth-Sun Lagrange point by DSCOVR/EPIC. *Geophysical Research Letters*, *45*, 11,456–11,464. https://doi.org/10.1029/2018GL079808

Received 2 AUG 2018
Accepted 9 OCT 2018
Accepted article online 15 OCT 2018
Published online 23 OCT 2018



# First Observations of Volcanic Eruption Clouds From the L1 Earth-Sun Lagrange Point by DSCOVR/EPIC

**S. A. Carn[1], N. A. Krotkov[2], B. L. Fisher[2,3], C. Li[2,4], and A. J. Prata[5]**

[1]Department of Geological and Mining Engineering and Sciences, Michigan Technological University, Houghton, MI, USA, [2]Atmospheric Chemistry and Dynamics Laboratory, Code 614, NASA Goddard Space Flight Center, Greenbelt, MD, USA, [3]Science Systems and Applications, Inc., Lanham, MD, USA, [4]Earth System Science Interdisciplinary Center, University of Maryland, College Park, MD, USA, [5]AIRES Pty Ltd, Melbourne, Victoria, Australia

**Abstract** Volcanic sulfur dioxide ($SO_2$) emissions have been measured by ultraviolet sensors on polar-orbiting satellites for several decades but with limited temporal resolution. This precludes studies of key processes believed to occur in young (~1–3 hr old) volcanic clouds. In 2015, the launch of the Earth Polychromatic Imaging Camera (EPIC) aboard the Deep Space Climate Observatory (DSCOVR) provided an opportunity for novel observations of volcanic eruption clouds from the first Earth-Sun Lagrange point (L1). The L1 vantage point provides continuous observations of the sunlit Earth, offering up to eight or nine observations of volcanic $SO_2$ clouds in the DSCOVR/EPIC field of view at ~1-hr intervals. Here we demonstrate DSCOVR/EPIC's sensitivity to volcanic $SO_2$ using several volcanic eruptions from the tropics to midlatitudes. The hourly cadence of DSCOVR/EPIC observations permits more timely measurements of volcanic $SO_2$ emissions, improved trajectory modeling, and novel analyses of the temporal evolution of volcanic clouds.

**Plain Language Summary** Satellite measurements of sulfur dioxide ($SO_2$) and ash emissions by volcanic eruptions are crucial for assessment of volcanic impacts on climate and mitigation of hazards to aviation. Until recently, the vast majority of such observations were made using satellites in *low-Earth* (or polar) orbit at altitudes of ~700–800 km, which only provide one measurement per day at most latitudes. This precludes studies of dynamic processes in volcanic clouds, which could radically alter their composition and potential impact. Here we report the first measurements of volcanic $SO_2$ emissions from an entirely new perspective: the Earth Polychromatic Imaging Camera (EPIC) aboard the Deep Space Climate Observatory, located at the first Earth-Sun Lagrange point (L1), 1.6 million kilometers from Earth. From L1, EPIC views the sunlit Earth continuously as it rotates and can measure volcanic $SO_2$ hourly from sunrise to sunset, as we demonstrate using several recent volcanic eruptions as examples. EPIC measurements allow us to detect volcanic eruptions sooner, and track their emissions for longer, than was previously possible with a single sensor. Our paper thus demonstrates a new Earth observation paradigm that could revolutionize studies of volcanic cloud chemistry and impacts and potentially reduce the societal impacts of volcanic eruptions.

## 1. Introduction

Most Earth observation from space is currently performed using satellites in polar (low Earth, LEO) or geostationary (GEO) orbit. LEO sensors can provide high spatial resolution (meter scale or better) observations and global coverage including the polar regions at low (~daily) temporal frequency. GEO sensors offer high temporal resolution (approximately minutes) but lower spatial resolution (kilometer scale) and coverage of one hemisphere from low to subpolar latitudes. Hence, GEO orbits support time-critical applications (e.g., monitoring of severe weather) but LEO orbits are needed for global coverage and analyses requiring high spatial resolution.

Both LEO and GEO orbits are used for the detection and mapping of volcanic eruption clouds, with two primary goals: detection and characterization of volcanic ash clouds for aviation safety (mainly GEO; e.g., Pavolonis et al., 2013) and measurement of sulfur dioxide ($SO_2$) emissions to assess volcanic impacts on the atmosphere and climate (mainly LEO; e.g., Carn et al., 2016). Although some operational GEO thermal infrared imagers can detect volcanic $SO_2$ (e.g., Prata & Kerkmann, 2007), most $SO_2$ measurements are collected from LEO ultraviolet (UV) and thermal infrared sensors, with low temporal resolution. This has limited studies of several processes that may impact the sulfur burden in fresh volcanic clouds during the first few hours of atmospheric residence, including the interaction of ash, ice (or hydrometeors), and gas; emission

and oxidation of other sulfur gas species (e.g., hydrogen sulfide, $H_2S$); and early (or primary) sulfate aerosol formation (e.g., Rose et al., 2000). Rose et al. (2000) noted that detailed evaluation of such processes required improved data frequency, especially in the UV.

The 2015 deployment of the Earth Polychromatic Imaging Camera (EPIC) aboard the Deep Space Climate Observatory (DSCOVR), located at the first Earth-Sun Lagrange point (L1) ~1.6 million kilometers from Earth, provides a rare opportunity to explore a new Earth observation paradigm. The L1 vantage point enables a continuous view of the sunlit face of the Earth during its daily rotation. EPIC, is a 10-channel UV-near infrared spectroradiometer that provides sunrise-to-sunset Earth observations with a temporal cadence of 68–110 min depending on season (http://epic.gsfc.nasa.gov)), the highest temporal resolution of UV satellite measurements achieved to date. Calibrated EPIC radiances are available for retrievals of atmospheric trace gases including ozone ($O_3$) and $SO_2$ (Herman et al., 2018; Marshak et al., 2018). EPIC provides coverage of the entire sunlit Earth disk (including the polar regions in the summer months, unlike GEO sensors), partly fills a ~4-hr daytime measurement gap between overpasses of Sun-synchronous LEO assets at ~9:30 a.m. (e.g., the European MetOp-A/B satellites) and ~1:30 p.m. local time (e.g., NASA's Aqua, Aura, and Suomi-NPP satellites), and also collects data later into the afternoon. Here we present the first EPIC retrievals of $SO_2$ columns following several recent volcanic eruptions (Table 1) and demonstrate the potential of these unique observations to advance our understanding of volcanic cloud processes and impacts. We highlight several key advantages of observations from L1, including more timely eruption detection, improved constraints on initial eruptive $SO_2$ mass loading, and the potential for characterization of short-term trends in eruption intensity.

## 2. The EPIC Instrument

EPIC is a UV-near infrared spectroradiometer that captures 10 spectral exposures (using narrowband filters at wavelengths of 317.5, 325, 340, 388, 443, 551, 680, 688, 764, and 779.5 nm) of the sunlit Earth disk approximately every hour (mid-April to mid-October) or every 2 hr (rest of the year) using a 2,048 × 2,048 pixel charge-coupled device detector with a maximum signal-to-noise ratio of 290:1 (Herman et al., 2018). The spectral resolutions (full widths at half maximum) of the four UV filters (317.5–388 nm) are 1.0, 1.0, 2.7, and 2.6 nm, respectively. In the UV channels, charge-coupled device pixels are binned to yield an effective image size of 1,024 × 1,024 pixels, corresponding to a ground pixel size of about 18 × 18 $km^2$ near the image center. EPIC uses rotating filter wheels to select wavelengths, with a 30-s time lag between each exposure that means individual channels are not colocated. A correction procedure is applied to the EPIC Level 1b radiances to adjust the channel images to a common latitude-longitude grid with an accuracy of one fourth of a pixel (Herman et al., 2018). Daily EPIC images of Earth are available on the EPIC website (http://epic.gsfc.nasa.gov), where the geographical extent of the data throughout the year can be seen. Herman et al. (2018) and Marshak et al. (2018) provide more details on the EPIC characteristics and its applications.

## 3. The EPIC $SO_2$ Algorithm

We have developed a discrete band backscattered UV $SO_2$ algorithm (MS_SO2) that provides consistent $SO_2$ retrievals across the multiple UV satellite missions deployed since the first Total Ozone Mapping Spectrometer (Krueger et al., 1995, 2000). In the EPIC version of MS_SO2, the four EPIC UV channels (centered at wavelengths [$\lambda$] of 317.5, 325, 340, and 388 nm) are used to retrieve a state vector containing four atmospheric parameters: $SO_2$ column, $O_3$ column, the scene reflectivity (R) at 388 nm (which assumes that the observed radiance is Lambertian, or independent of viewing angle), and the spectral reflectivity dependence, $dR/d\lambda$.

The retrieval is performed in two steps, referred to here as Step 1 and Step 2. In Step 1, the four-element state vector, $\mathbf{x}$, is retrieved by inverting a 4 × 4 weighting matrix, $K$:

$$\mathbf{y} = K\mathbf{x} \tag{1}$$

where $\mathbf{y}$ is a four-element vector containing the four measured UV radiances. The weighting coefficients $K_{i,j}$ are defined by the respective sensitivities (or Jacobians) computed from a forward radiative transfer model for each state variable $x_j$:

$$K_{i,j} = \frac{\partial N_i}{\partial x_j}. \tag{2}$$

**Table 1**
*Volcanic Eruptions Detected by EPIC (June 2015 to July 2018)*

| Volcano | Eruption time (UTC) | First EPIC detection (UTC) | Difference (hr)[a] | EPIC exposures[b] | Maximum $SO_2$ column (DU) |
|---|---|---|---|---|---|
| Etna (Italy) | 3 Dec 2015, at 02:30 | 3 Dec at 08:16 | 5.77 | 3 | 46 |
| Bromo (Indonesia) | 2 Jan 2016 | 2 Jan at 04:09 | — | 3 | 38 |
| Pavlof (USA) | 27 Mar 2016, at 23:53 | 28 Mar at 21:54 | 22.02 | 2 | 25 |
| Aso-san (Japan) | 7 Oct 2016, at 16:46 | 8 Oct at 00:55 | 8.15 | 4 | 33 |
| Bogoslof (USA) | 8 Mar 2017, at 07:36 | 8 Mar at 20:15 | 12.65 | 3 | 29 |
| Kambalny (Russia) | 24 Mar 2017, at 21:20 | 25 Mar at 02:43 | 5.38 | 4 | 18 |
| Bogoslof (USA) | 28 May 2017, at 22:16 | 29 May at 01:23 | 3.12 | 4 | 38 |
| Tinakula (Solomon Is) | 20 Oct 2017, at 19:20 | 20 Oct at 20:53 | 1.55 | 5 | 68 |
| Agung (Indonesia) | 26 Nov 2017 | 27 Nov at 03:53 | — | 1 | 28 |
| Sinabung (Indonesia) | 19 Feb 2018, at 01:53 | 19 Feb at 03:53 | 2 | 4 | 74 |
| Ambae (Vanuatu) | 24 Mar 2018 | 24 Mar at 00:55 | — | 3 | 82 |
| Ambae (Vanuatu) | 6 Apr 2018 | 6 Apr at 01:04 | — | 3 | 71 |
| Fuego (Guatemala) | 3 Jun 2018, at 17:30[c] | 3 Jun at 18:03[d] | 0.55 | 3 | 37 |
| Fernandina (Ecuador) | 16 Jun 2018, at 17:00 | 16 Jun at 19:28 | 2.47 | 7 | 44 |
| Sierra Negra (Ecuador) | 26 Jun 2018, at 19:40 | 26 Jun at 21:57 | 2.28 | 8–9 | 91 |
| Ambae (Vanuatu) | 26 Jul 2018 at 10:00 | 26 Jul at 20:24 | 10.4 | 4 | 221 |

*Note.* EPIC = Earth Polychromatic Imaging Camera; DU = Dobson units.
[a]Only given if eruption start time is known. [b]Maximum number of consecutive EPIC exposures containing volcanic $SO_2$. [c]Onset of largest explosive eruption as reported by the Washington Volcanic Ash Advisory Center (Global Volcanism Program, 2018). [d]Aerosol Index (AI) signal indicating volcanic ash.

where $N_i$ is the forward model calculated $N$ value ($N = -100 \log_{10} [I/F]$, where $I$ = Top of Atmosphere radiance and $F$ = incoming solar irradiance) at each of the four UV wavelengths, $i$. To calculate the $SO_2$ sensitivities ($\partial N/\partial SO_2$), we assume the $SO_2$ plume has a Gaussian vertical profile centered at 13-km altitude with a standard deviation of 2 km.

The EPIC channel geolocation errors described above produce noise in the Step 1 retrievals, which we correct for by implementing a Step 2 procedure. In Step 2, we first apply a 31 × 31 mean filter to smooth the entire Step 1 retrieved $O_3$ field, and then perform a second retrieval using the Step 1 retrieved quantities as first guesses. The $O_3$ and reflectivity remain fixed in Step 2, resulting in a two-parameter retrieval of $SO_2$ and $dR/d\lambda$. A UV Aerosol Index (AI) sensitive to volcanic ash, which can also be used to detect volcanic eruptions (e.g., Table 1), is calculated as: $AI = dR/d\lambda * dN/dR^*(N_{340} - N_{388})$.

As we demonstrate below, the EPIC $SO_2$ algorithm has adequate sensitivity to detect moderate to large volcanic eruptions (Table 1) when the $SO_2$ column in an EPIC pixel exceeds ~5–15 Dobson units (1 DU = $2.68 \times 10^{16}$ molecules/cm$^2$). Although hyperspectral UV instruments such as the Ozone Monitoring Instrument (OMI) and Ozone Mapping and Profiler Suite (OMPS) have higher $SO_2$ sensitivity (e.g., Carn et al., 2016), the EPIC observations have the benefit of higher cadence. There are several potential sources of error on the EPIC $SO_2$ retrievals, including aerosols (e.g., volcanic ash or sulfate aerosol) and an incorrect $SO_2$ altitude. Radiative transfer calculations suggest maximum errors of ±30% for $SO_2$ plumes located within ±2 km of the assumed altitude (13 km), with larger errors at high latitudes. Potential errors due to high aerosol loadings have not yet been assessed but could be significant in fresh, ash-rich eruption clouds.

## 4. Results

No major (stratospheric) eruptions have occurred since June 2015. However, there have been several smaller eruptions from equatorial (Galápagos Islands, Ecuador) to high latitudes (Alaska), permitting evaluation of EPIC's sensitivity to common volcanic events under a range of observing conditions (Table 1). To date a maximum of eight to nine EPIC consecutive exposures of a volcanic $SO_2$ cloud in ~8 hr has been achieved, after the eruption of Sierra Negra (Galápagos Islands, Ecuador) in June 2018. Several other eruptions have been captured in four to seven EPIC exposures (Table 1). Here we focus on three recent eruptions that demonstrate the advantages of these high-cadence UV observations from L1: the May 2017 eruption of Bogoslof (Alaska, USA), the October 2017 eruption of Tinakula (Solomon Islands), and the June 2018 eruption of Sierra Negra.

### 4.1. The 28–29 May 2017 Eruption of Bogoslof (AK, USA)

Bogoslof (AK, USA; 53.93°N, 168.03°W) is a largely submarine volcano in the Aleutian Islands that produced a series of 64 explosive eruptions between December 2016 and August 2017 (http://www.avo.alaska.edu). At least two of these eruptions (8 March and 28 May 2017) were detected by EPIC (Table 1). The 28 May 2017 eruption began at 22:16 UTC (14:16 AKDT) and lasted 50 min, injecting a volcanic ash cloud to altitudes of at least 12 km (a Volcanic Explosivity Index [VEI] of 3; Global Volcanism Program, 2013) and generating significant volcanic lightning detected by the World Wide Lightning Location Network at 22:40–23:01 UTC. As expected for a partly submerged vent, the initial eruption column was observed to be very water-rich in visible satellite imagery (e.g., https://avo.alaska.edu/images/image.php?id=109261), raising the possibility of $SO_2$ scavenging and/or rapid sulfate aerosol production in the volcanic plume.

Volcanic $SO_2$ emitted by the Bogoslof eruption was captured in four EPIC exposures from 01:23 to 04:39 UT on 28 May (Figure 1), beginning ~3 hr after the eruption onset (Table 1). The sequence of EPIC images (Figure 1) reveals slow movement of the $SO_2$ cloud away from the volcano over ~3 hr, indicating low wind speeds (consistent with the closest available radiosonde sounding; supporting information Figure S1) and consequently low wind shear. Since high wind shear could reduce $SO_2$ columns below the EPIC detection limit, these conditions are favorable for geophysical interpretation of $SO_2$ mass variations.

Coincident thermal infrared data from the GOES-15 (GOES-W) satellite show ~N-NE transport of an opaque volcanic cloud (Figures 1 and S2). Geostationary satellite data suffer from parallax effects (e.g., Johnson et al., 1994) that displace objects away from the subsatellite point (135°W for GOES-W), but we have corrected for this in Figure 2 using a normalized cloud offset (http://www-das.uwyo.edu/~geerts/cwx/notes/chap02/parallax.html). For a cloud at 11–15 km altitude and 54°N, the parallax offset is ~20–30 km, which we confirmed by comparing a visible LEO Suomi National Polar-orbiting Partnership (SNPP) Visible Infrared Imaging Radiometer Suite (VIIRS) image of the volcanic cloud at 23:35 UTC with the uncorrected GOES-W image at 23:30 UTC. Note that while EPIC also suffers from parallax effects, they are negligible in this case due to DSCOVR's much greater distance from Earth and the Northern Hemisphere location of the subsatellite point in late May (close to the summer solstice). The parallax-corrected GOES-W data and near-coincident EPIC $SO_2$ retrievals (Figure 1) reveal a clear separation of the hydrometeor/ash and $SO_2$-rich portions of the volcanic cloud, with the $SO_2$ at higher altitude (since it is not obscured by the opaque cloud). Radiosonde data (Figure S1) suggests an altitude of 12–13 km for the $SO_2$ cloud. Rose et al. (2000) speculated on several mechanisms to explain this separation of ash and gas in volcanic clouds, including dynamic separation, pre-eruptive gas segregation, or $SO_2$ scavenging. The Bogoslof data show EPIC's potential to provide more observational constraints on this phenomenon and elucidate the processes involved (e.g., in conjunction with plume modeling; Prata et al., 2017).

The EPIC $SO_2$ data for Bogoslof also reveal a transient $SO_2$ feature in the 02:28 UT exposure, distinct from the main $SO_2$ cloud and the opaque cloud detected by GOES-W (Figure 1b). Release of $SO_2$ from sublimating ice (e.g., Textor et al., 2003) or oxidation of $H_2S$ are potential sources for this transient gas. Possible sources of $H_2S$ in the Bogoslof emissions include magmatic gas (e.g., Aiuppa et al., 2005) or magma-water interactions in the aqueous environment of the vent (e.g., Clarisse et al., 2011). The rate constant for reaction of the OH radical with $H_2S$ is an order of magnitude larger than its reaction with $SO_2$, hence oxidation of $H_2S$ to $SO_2$ should proceed more rapidly than conversion of $SO_2$ to sulfate aerosol (e.g., Graedel, 1977; Rose et al., 2000). We also note that SNPP/OMPS measured ~7–8 kt of $SO_2$ in the Bogoslof volcanic cloud ~19 hr later on 29 May at 23:15–23:20 UT (Figure S3), indicating no significant $SO_2$ loss on this timescale. This would be consistent with production of $SO_2$ (e.g., via oxidation of $H_2S$) dominating (or compensating for) $SO_2$ loss during this period.

### 4.2. The 20 October 2017 Eruption of Tinakula (Solomon Islands)

The October 2017 eruption of remote Tinakula volcano was relatively small (VEI ~3) yet among the largest eruptions of that year. The eruption consisted of two explosive events: the first began at around 19:20 UT on 20 October, injecting an ash plume to 4.6-km altitude, followed by a second ash-producing eruption at 23:40 UT that reached 10.7-km altitude and generated a visible shock wave (Global Volcanism Program, 2017). EPIC detected $SO_2$ emissions from the first eruption at 20:53 UT on 20 October, less than 2 hr after the onset (Table 1 and Figure 2), and the subsequent EPIC exposure (22:41 UT) measured ~14 kt of $SO_2$ in the eruption cloud. The next EPIC measurement (00:55 UT, 21 October) occurred ~80 min after the second

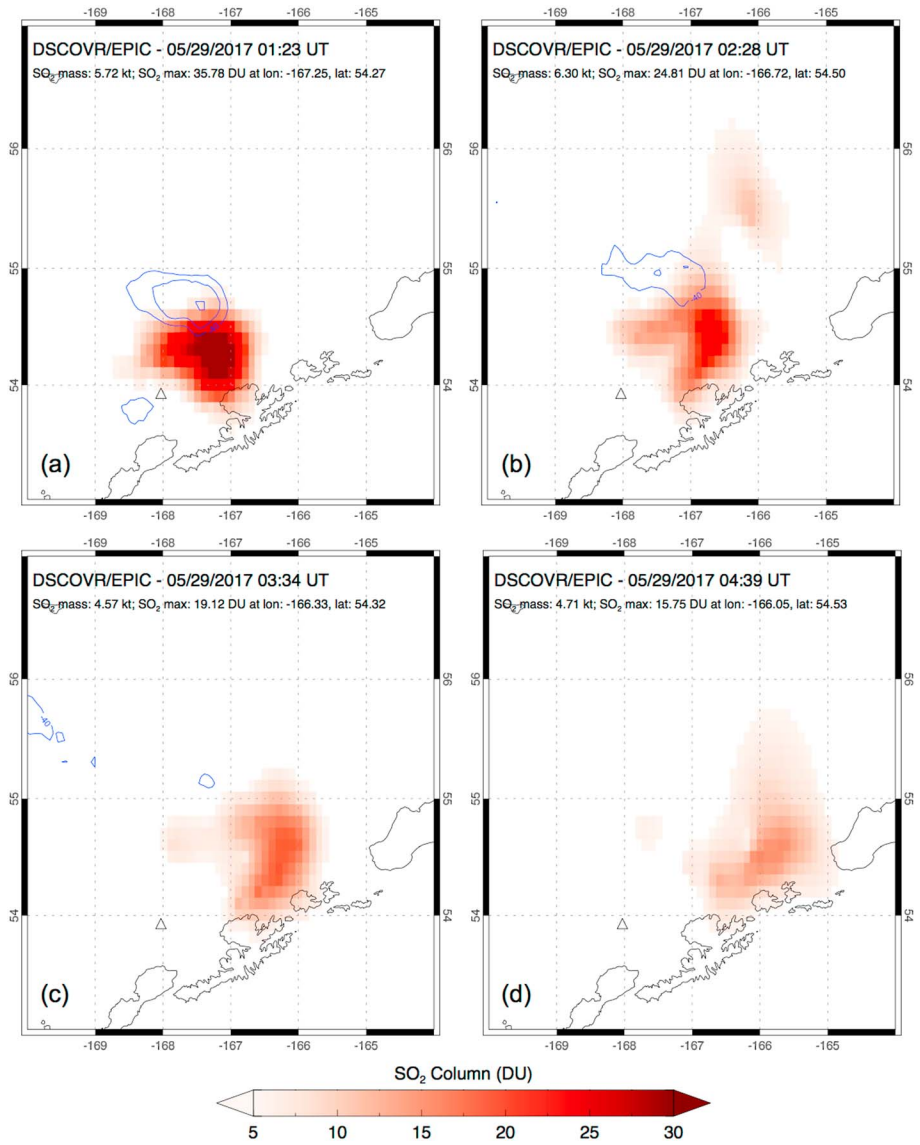


**Figure 1.** Four consecutive EPIC $SO_2$ maps for the 28–29 May 2017 eruption of Bogoslof volcano (AK, USA; *triangle*). The eruption occurred at 22:16 UTC on 28 May (Table 1). $SO_2$ in the Bogoslof volcanic cloud was detected in four EPIC exposures on 29 May at (a) 01:23 UTC, (b) 02:38 UTC, (c) 03:34 UTC, and (d) 04:39 UTC. The EPIC retrievals show the relatively slow movement of the $SO_2$ cloud to the northeast. The *blue contours* shown in a–c denote regions of infrared brightness temperatures $\leq -40$ °C derived from near-coincident GOES-15 geostationary infrared data. These demarcate the boundary of an opaque, ice-rich volcanic cloud (likely also containing ash) which is separate from (below) the $SO_2$ cloud. EPIC = Earth Polychromatic Imaging Camera.

explosive event (when we assume some residual $SO_2$ from the first eruption remained) but did not detect an increase in $SO_2$ loading (Figure 2). At ~02:20 UT overpasses of the LEO UV sensors (OMI and OMPS) measured the merged $SO_2$ loading from both eruptive events, which were also observed in later EPIC exposures but which remained below the ~14 kt measured at 22:41 UT on 20 October (Figure 2). Thus, in this case the EPIC observations permit distinction between emissions from two separate eruptions, indistinguishable in the LEO data, and suggest that the first eruptive event likely discharged most of the $SO_2$. Such attribution of gas emissions during eruptions with multiple phases is important for understanding volcanic processes such as pre-eruptive gas accumulation.

The lower $SO_2$ sensitivity of EPIC relative to hyperspectral LEO UV sensors such as OMI is apparent in Figure 2. OMI measured a higher total $SO_2$ loading at 02:23 UT (~20 kt) than EPIC at 02:43 UT (~11 kt), since EPIC lacks

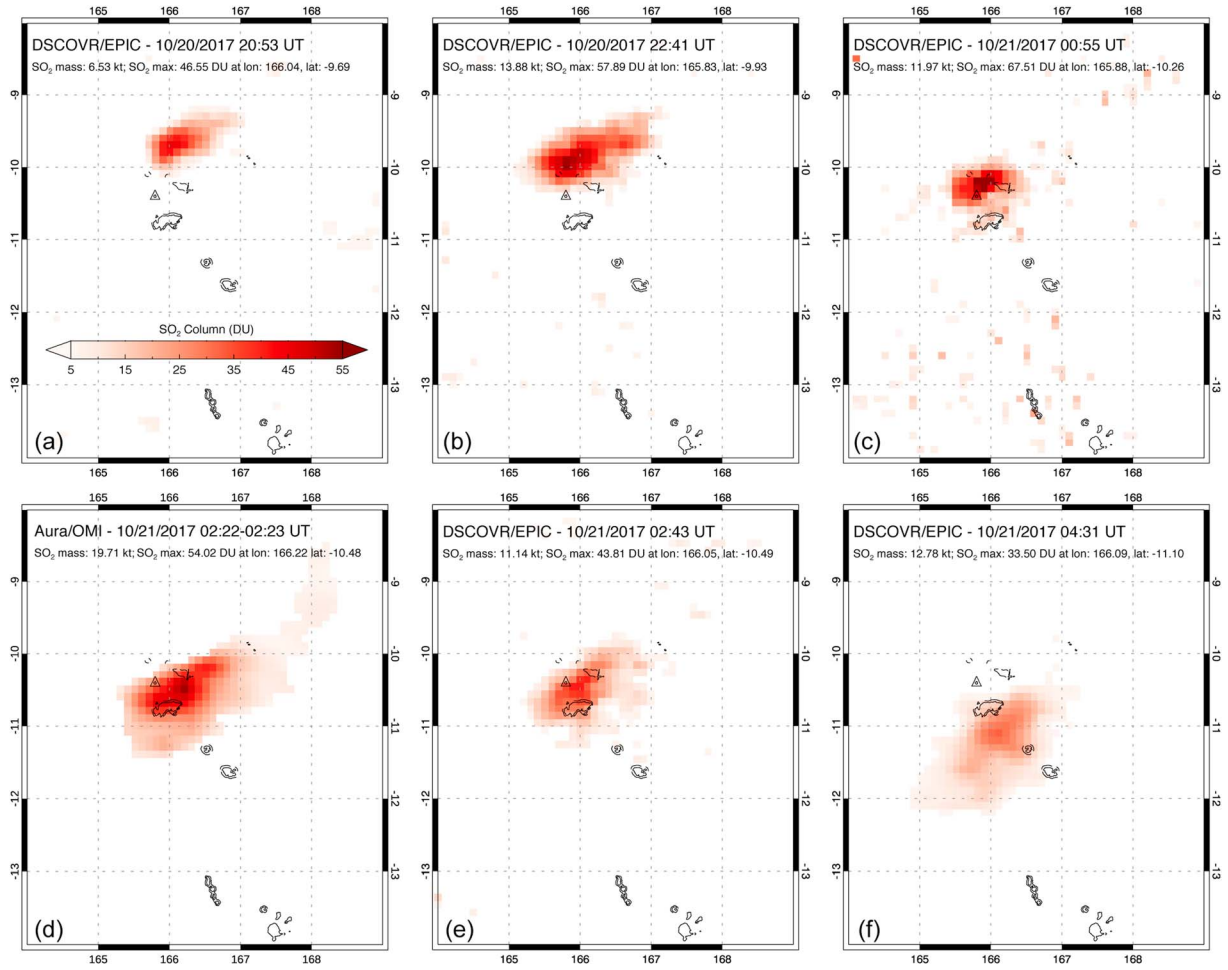


**Figure 2.** Five consecutive EPIC $SO_2$ images for the 20–21 October 2017 eruption of Tinakula volcano (Solomon Islands; *triangle*). Two separate eruptions occurred at 19:20 and 23:40 UT on 20 October (Table 1). $SO_2$ was detected in EPIC exposures at (a) 20:53 UTC 20 Oct, (b) 22:41 UT 20 Oct, (c) 00:55 UT 21 Oct, (e) 02:43 UT 21 Oct, and (f) 04:31 UT 21 Oct. All EPIC images use the color scale shown in a. Panel (d) shows a LEO Aura/OMI principal component analysis algorithm $SO_2$ retrieval (Li et al., 2017) at 02:23 UT on 21 Oct, using the same color scale as the EPIC maps. EPIC = Earth Polychromatic Imaging Camera; LEO = satellite in low Earth orbit; OMI = Ozone Monitoring Instrument.

sensitivity to the lower $SO_2$ columns near the periphery of the volcanic cloud (Figure 2). However, the comparison shows that the EPIC retrievals are in good agreement (in terms of location and $SO_2$ column) with OMI in the core of the $SO_2$ cloud and provide important context for the LEO observations. We reiterate that the 2017 Tinakula eruption was relatively small, and we expect EPIC to provide optimal data when the next major stratospheric volcanic eruption occurs.

### 4.3. The June 2018 Eruption of Sierra Negra (Galápagos Islands, Ecuador)

Two Galápagos Island eruptions in June 2018 provided the best demonstration yet of the advantages of high-cadence EPIC observations. Fernandina volcano (Isla Fernandina) began a short (2–3 day) eruption on 16 June 2018, then Sierra Negra (Isla Isabela) erupted on 26 June, continuing into July. Both eruptions were captured in seven to nine consecutive EPIC exposures (Table 1) due to the favorable equatorial location. We focus here on the Sierra Negra eruption, but animations of EPIC $SO_2$ data for both events are provided as supporting information (Movies S1, S2, and S3). Both eruptions were predominantly effusive events with low VEIs of 1–2 (Global Volcanism Program, 2013).

The Sierra Negra eruption began at 19:40 UT on 26 June, and an SNPP/OMPS overpass ~30 min later at 20:09 UT measured a small amount of $SO_2$ (~0.5 kt), though insufficient to be deemed a significant eruption. However, a late afternoon EPIC exposure at 21:57 UT detected high $SO_2$ column amounts (~90 DU)

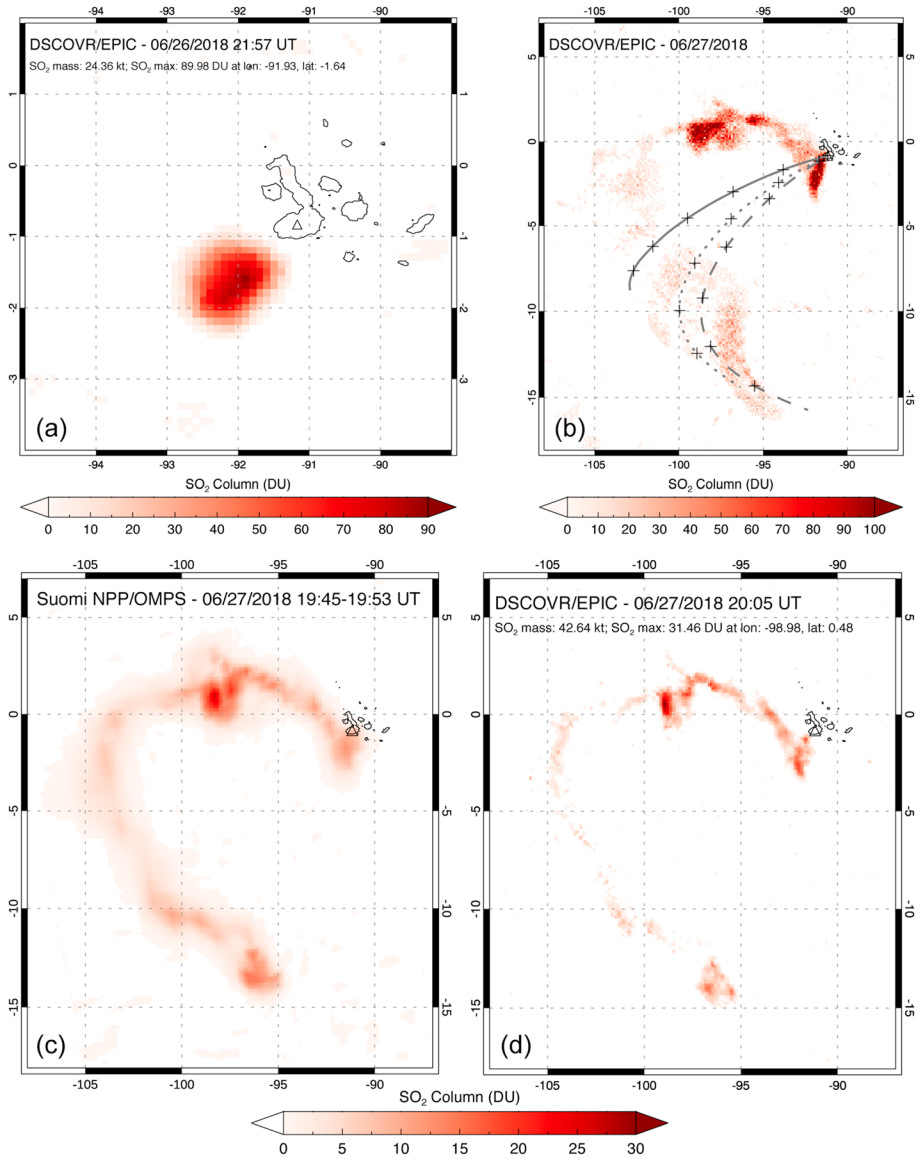


**Figure 3.** (a) EPIC detection of strong $SO_2$ emissions from Sierra Negra (Galápagos Islands; *triangle*) at 21:57 UT on 26 June 2018; (b) cumulative $SO_2$ column amounts measured in the Sierra Negra volcanic plume by EPIC in eight exposures on 27 June 2018 (14:38–22:16 UT). *Dashed*, *dotted*, and *solid lines* show 36-hr HYSPLIT model forward trajectories for an eruption to altitudes of 11, 12, and 13 km, respectively, beginning at 19:00 UT on 26 June, with *crosses* every 6 hr. (c) SNPP/OMPS map of $SO_2$ emissions from sierra Negra at 19:50 UT on June 27 (maximum $SO_2$ column is 27 DU); d EPIC $SO_2$ map at 20:05 UT on June 27 (maximum $SO_2$ column is 31 DU). Panels (c) and (d) use the same color scale. EPIC = Earth Polychromatic Imaging Camera; HYSPLIT = HYbrid Single Particle Lagrangian Integrated Trajectory; OMPS = Ozone Mapping and Profiler Suite.

southwest of the volcano (Figure 3), indicative of a significant eruption in progress. On 27 June, EPIC observations were available at peak hourly cadence and the Sierra Negra $SO_2$ cloud was detected in eight to nine consecutive exposures (Figure 3 and supporting information Movie S2), which is probably the maximum achievable. Figure 3b shows the cumulative $SO_2$ amount detected in these exposures, and nicely captures the curved trajectory of a parcel of $SO_2$ transported to the south. We attempted to fit HYbrid Single Particle Lagrangian Integrated Trajectory (HYSPLIT) model (Rolph et al., 2017; Stein et al., 2015) trajectories to the EPIC $SO_2$ data. Trajectories initialized over Sierra Negra at 19:00 UT on 26 June at altitudes of 11–13 km provided the best match with $SO_2$ detected by EPIC southwest of the volcano (Figure 3b); discrepancies may be due to insufficient meteorological data driving the HYSPLIT model in the

region. $SO_2$ loadings measured in the consecutive EPIC exposures on 27 June shows a steady decline over the ~8-hr period from ~55 kt at 14:38 UT to ~27 kt at 22:16 UT (supporting information Movie S2). Most of this variation is probably due to changing $SO_2$ sensitivity as the EPIC viewing geometry and solar zenith angle (SZA) changes, but it is clear that there were no further significant $SO_2$ emissions from Sierra Negra in this time frame. Hence, unlike LEO sensors, the EPIC observations can potentially provide information on hourly trends in eruption intensity, although this will require further analysis of how sensitivity varies with observation geometry.

In Figure 3 we also show a SNPP/OMPS $SO_2$ measurement using the principal component analysis algorithm (Li et al., 2017) made close to the time of one EPIC exposure. As for Tinakula, this shows the lower sensitivity of EPIC relative to the hyperspectral UV instruments but nevertheless demonstrates the consistency between EPIC and OMPS $SO_2$ columns in the core region of the volcanic cloud. And unlike the single OMPS $SO_2$ image, the sequence of EPIC observations provides unique information on cloud transport and short-term trends in eruption intensity (Figure 3 and supporting information Movies S2 and S3).

## 5. Discussion

Our results demonstrate that EPIC has sufficient $SO_2$ sensitivity (~5–10 DU) to detect all significant volcanic eruptions that occur within its field of view (FOV). However, EPIC's unique advantage over LEO satellite instruments is the higher cadence of $SO_2$ observations. Continuous eruptions (e.g., Sierra Negra in June 2018), or eruptions that begin as the volcano rotates into the EPIC FOV, will yield the maximum number of daily EPIC observations, albeit with varying SZA. The Galápagos Islands eruptions in June 2018 (Table 1) show that at least seven to eight EPIC exposures over a period of several hours can be obtained, potentially revealing short-term trends in volcanic emissions. Future work will quantify the impact of varying observing conditions (e.g., SZA) on EPIC's $SO_2$ detection limit and retrieval uncertainties.

EPIC offers the potential for rapid detection of eruptions within its FOV and for assessment of eruption evolution on hourly timescales, which would be advantageous for volcanic hazard mitigation. EPIC currently has no near-real-time data capability as only two antennae (in Virginia and Alaska, USA) are used for downlink to Earth and only receive data when in view of DSCOVR (Herman et al., 2018). This could be remedied by installation of more receivers, such that at least one antenna is always within the EPIC FOV. But regardless of near-real-time capabilities, early detection of volcanic clouds is critical for accurate assessment of eruptive $SO_2$ emissions, particularly for major eruptions with potential climate impacts. LEO UV sensors often detect volcanic eruptions several hours, or close to a day, after the eruption onset, during which time the emitted $SO_2$ mass can change substantially. LEO $SO_2$ measurements can be extrapolated back to the time of eruption (e.g., Krotkov et al., 2010), but this requires a long time series of $SO_2$ loadings that take days to weeks to acquire. As shown here, EPIC has detected several eruptions within a few hours of their onset, and despite lower sensitivity than hyperspectral UV sensors EPIC's higher cadence provides context for LEO $SO_2$ measurements and allows us to gauge how representative the LEO data might be of the peak volcanic $SO_2$ loading. EPIC $SO_2$ observations would therefore also be of value for assimilation into climate models that predict volcanic impacts on climate.

## 6. Conclusions

The DSCOVR/EPIC instrument, in orbit at L1 since 2015, is a valuable addition to current spaceborne assets capable of detecting volcanic eruption clouds, providing unique UV observations of volcanic $SO_2$ with hourly cadence. Results presented here show that our EPIC $SO_2$ algorithm has detected every significant volcanic eruption since the DSCOVR launch. Although relatively small, these eruptions have demonstrated EPIC's sensitivity to moderate volcanic eruptions at a range of latitudes. EPIC should provide exceptional observations if still operational when the next major stratospheric volcanic eruption (VEI 4+) occurs. We have also demonstrated EPIC's ability to track volcanic cloud transport on hourly timescales; a significant advance over LEO UV sensors (e.g., OMI, OMPS). Preliminary comparisons of EPIC $SO_2$ retrievals with OMI and OMPS data indicate consistent $SO_2$ columns and loadings. It is clear that the EPIC observations have great potential to provide new insight into the short-term evolution of volcanic $SO_2$ clouds and also to enable more timely

detection of volcanic eruptions. The potential value of frequent UV observations of volcanic clouds has been noted in the past, and with EPIC this has become a reality.

**Acknowledgments**
We acknowledge NASA Earth Science Division support for development of the EPIC $SO_2$ products through grant NNX15AC61G (DSCOVR Earth Science Algorithms program; PI: N. A. Krotkov). EPIC Sulfur Dioxide data products are available at the Atmospheric Science Data Center (ASDC) at NASA Langley Research Center: https://eosweb.larc.nasa.gov/project/dscovr/dscovr_epic_l2_so2_01. The NOAA Air Resources Laboratory (ARL) is acknowledged for the provision of the HYSPLIT transport and dispersion model and/or READY website (http://www.ready.noaa.gov) used in this publication.

## References

Aiuppa, A., Inguaggiato, S., McGonigle, A. J. S., O'Dwyer, M., Oppenheimer, C., Padgett, M. J., et al. (2005). $H_2S$ fluxes from Mt. Etna, Stromboli, and Vulcano (Italy) and implications for the sulfur budget at volcanoes. *Geochimica et Cosmochimica Acta*, *69*(7), 1861–1871. https://doi.org/10.1016/j.gca.2004.09.018

Carn, S. A., Clarisse, L., & Prata, A. J. (2016). Multi-decadal satellite measurements of global volcanic degassing. *Journal of Volcanology and Geothermal Research*, *311*, 99–134. https://doi.org/10.1016/j.jvolgeores.2016.01.002

Clarisse, L., Coheur, P.-F., Chefdeville, S., Lacour, J.-L., Hurtmans, D., & Clerbaux, C. (2011). Infrared satellite observations of hydrogen sulfide in the volcanic plume of the August 2008 Kasatochi eruption. *Geophysical Research Letters*, *38*, L10804. https://doi.org/10.1029/2011GL047402

Global Volcanism Program (2013). *Volcanoes of the world*, v. 4.7.4. Venzke, E (Ed.). Washington, DC: Smithsonian Institution. Downloaded 04 Oct 2018. https://doi.org/10.5479/si. GVP.VOTW4-2013

Global Volcanism Program (2017). In S. K. Sennert (Ed.), Weekly Volcanic Activity Report, 18 October-24 October 2017 *Report on Tinakula (Solomon Islands)*. Washington, DC: Smithsonian Institution and US Geological Survey.

Global Volcanism Program (2018). In S. K. Sennert (Ed.), Weekly Volcanic Activity Report, 30 May-5 June 2018 *Report on Fuego (Guatemala)*. Washington, DC: Smithsonian Institution and US Geological Survey.

Graedel, T. E. (1977). The homogenous chemistry of atmospheric sulfur. *Reviews of Geophysics*, *15*(4), 421–428. https://doi.org/10.1029/RG015i004p00421

Herman, J., Huang, L., McPeters, R., Ziemke, J., Cede, A., & Blank, K. (2018). Synoptic ozone, cloud reflectivity, and erythemal irradiance from sunrise to sunset for the whole Earth as viewed by the DSCOVR spacecraft from the Earth-Sun Lagrange 1 orbit. *Atmospheric Measurement Techniques*, *11*(1), 177–194. https://doi.org/10.5194/amt-11-177-2018

Johnson, D. B., Flament, P., & Bernstein, R. L. (1994). High-resolution satellite imagery for mesoscale meteorological studies. *Bulletin of the American Meteorological Society*, *75*(1), 5–33. https://doi.org/10.1175/1520-0477(1994)075<0005:HRSIFM>2.0.CO;2

Krotkov, N. A., Schoeberl, M. R., Morris, G. A., Carn, S. A., & Yang, K. (2010). Dispersion and lifetime of the $SO_2$ cloud from the August 2008 Kasatochi eruption. *Journal of Geophysical Research*, *115*, D00L20. https://doi.org/10.1029/2010JD013984

Krueger, A. J., Schaefer, S. J., Krotkov, N., Bluth, G., & Barker, S. (2000). Ultraviolet remote sensing of volcanic emissions. In P. J. Mouginis-Mark, J. A. Crisp, & J. H. Fink (Eds.), *Remote sensing of active volcanism*, *Geophysical Monograph* (Vol. 116, pp. 25–43). Washington, DC: American Geophyical Union. https://doi.org/10.1029/GM116p0025

Krueger, A. J., Walter, L. S., Bhartia, P. K., Schnetzler, C. C., Krotkov, N. A., Sprod, I., & Bluth, G. J. S. (1995). Volcanic sulfur dioxide measurements from the total ozone mapping spectrometer instruments. *Journal of Geophysical Research*, *D100*, 14,057–14,076.

Li, C., Krotkov, N. A., Carn, S. A., Zhang, Y., Spurr, R. J. D., & Joiner, J. (2017). New-generation NASA Aura Ozone Monitoring Instrument volcanic $SO_2$ dataset: Algorithm description, initial results, and continuation with the Suomi-NPP Ozone Mapping and Profiler Suite. *Atmospheric Measurement Techniques*, *10*(2), 445–458. https://doi.org/10.5194/amt-10-445-2017.

Marshak, A., Herman, J., Szabo, A., Blank, K., Carn, S., Cede, A., et al. (2018). Earth observations from DSCOVR/EPIC instrument. *Bulletin of the American Meteorological Society*. https://doi.org/10.1175/BAMS-D-17-0223.1

Pavolonis, M., Heidinger, A., & Sieglaff, J. (2013). Automated retrievals of volcanic ash and dust cloud properties from upwelling infrared measurements. *Journal of Geophysical Research: Atmospheres*, *118*, 1436–1458. https://doi.org/10.1002/jgrd.50173

Prata, A. J., & Kerkmann, J. (2007). Simultaneous retrieval of volcanic ash and $SO_2$ using MSG-SEVIRI measurements. *Geophysical Research Letters*, *34*, L05813. https://doi.org/10.1029/2006GL028691

Prata, F., Woodhouse, M., Huppert, H. E., Prata, A., Thordarson, T., & Carn, S. (2017). Atmospheric processes affecting the separation of volcanic ash and $SO_2$ in volcanic eruptions: Inferences from the May 2011 Grímsvötn eruption. *Atmospheric Chemistry and Physics*, *17*(17), 10,709–10,732. https://doi.org/10.5194/acp-17-10709-2017

Rolph, G., Stein, A., & Stunder, B. (2017). Real-time Environmental Applications and Display sYstem: READY. *Environmental Modelling & Software*, *95*, 210–228. https://doi.org/10.1016/j.envsoft.2017.06.025

Rose, W. I., Bluth, G. J. S., & Ernst, G. G. J. (2000). Integrating retrievals of volcanic cloud characteristics from satellite remote sensors: A summary. *Philosophical transactions of the Royal Society of London. Series: A*, *358*(1770), 1585–1606. https://doi.org/10.1098/rsta.2000.0605

Stein, A. F., Draxler, R. R., Rolph, G. D., Stunder, B. J. B., Cohen, M. D., & Ngan, F. (2015). NOAA's HYSPLIT atmospheric transport and dispersion modeling system. *Bulletin of the American Meteorological Society*, *96*(12), 2059–2077. https://doi.org/10.1175/BAMS-D-14-00110

Textor, C., Graf, H.-F., Herzog, M., & Oberhuber, J. M. (2003). Injection of gases into the stratosphere by explosive volcanic eruptions. *Journal of Geophysical Research*, *108*(D19), 4606. https://doi.org/10.1029/2002JD002987